F. Caccia, L. Abergo, A. Savino, M. Morelli, B.Y. Zhou, G. Gori, A. Zanotti, G. Gibertini, L. Vigevano, A. Guardone
Multi-Fidelity Numerical Approach to Aeroacoustics of Tandem Propellers in eVTOL Airplane Mode
in: AIAA Aviation 2023 Forum, AIAA, 2023, ISBN: 9781624107047, p. 1-14, AIAA 2023-3221
[AIAA Aviation 2023 Forum, San Diego, CA, USA, 12-16 June 2023]
doi:10.2514/6.2023-3221

The final publication is available at https://doi.org/10.2514/6.2023-3221

Multi-Fidelity Numerical Approach to Aeroacoustics of Tandem Propellers in eVTOL Airplane Mode

Francesco Caccia*, Luca Abergo†, Alberto Savino‡ and Myles Morelli§
Department of Aerospace Science and Technology, Politecnico di Milano
Building B12, Via La Masa 34, Milano, MI 20156, Italy

Beckett Y. Zhou¶
Department of Aerospace Engineering, University of Bristol
Building, University Walk, Bristol, BS8 1TR, United Kingdom

Giulio Gori ‖, Alex Zanotti**, Giuseppe Gibertini ††, Luigi Vigevano‡‡ and Alberto Guardone§§
Department of Aerospace Science and Technology, Politecnico di Milano
Building B12, Via La Masa 34, Milano, MI 20156, Italy

The present paper deals with an innovative multi-fidelity framework for characterizing the aerodynamics and the aeroacoustics of multirotor systems with application to advanced eVTOL aircraft. In this framework, the goal of the activity is a multi-fidelity investigation of two propellers in tandem with rotor disks overlap, reproducing a typical feature of eVTOL architectures in airplane mode flight conditions. A Ffowcs Williams–Hawkings equation solver is used to compute the aeroacoustic footprint of the test case in different configurations. The solver is run with both mid-fidelity aerodynamic simulation data obtained with DUST and high-fidelity simulation data obtained with SU2. The comparison between the two different approaches highlights the suitability of the DUST mid-fidelity simulations for the aeroacoustic investigation of a propeller in airplane mode configuration with a much lower computational cost with respect to high-fidelity CFD simulations. On the other hand, the co-axial propellers tandem configuration shows some differences in the sound pressure level computed with the two approaches, mainly due to the contribution to noise emission given by the rear propeller.

Nomenclature

C_P	=	power coefficient [-]
C_T	=	thrust coefficient [-]
D	=	propeller diameter [m]
J	=	Advance ratio [-]
L_x	=	axial distance between propellers disks [m]
L_y	=	lateral distance between propellers rotation axis [m]
M	=	Mach number [-]
n	=	rotor speed [rev/s]
P	=	Pressure [Pa]
R	=	propeller radius [m]

*PhD student, francescoangelo.caccia@polimi.it
†PhD student, luca.abergo@polimi.it
‡PhD student, alberto.savino@polimi.it
§Postdoctoral Researcher, mylescarlo.morelli@polimi.it
¶Assistant Professor, beckett.zhou@bristol.ac.uk
‖Assistant Professor, giulio.gori@polimi.it
**Associate Professor, alex.zanotti@polimi.it
††Associate Professor, giuseppe.gibertini@polimi.it
‡‡Associate Professor, luigi.vigevano@polimi.it
§§Full Professor, alberto.guardone@polimi.it

SPL = Sound Pressure Level [dB]
T = Thrust [N]
U_∞ = Free-stream velocity [$\mathrm{m\,s^{-1}}$]
β = Pitch angle [°]
θ = Temperature [K]
ρ = Free-stream air density [$\mathrm{kg\,m^{-3}}$]
φ = Microphone angular position [°]
Ω = rotor speed [RPM]
ω = vorticity [Hz]

I. Introduction

Urbanization, and the rapidly growing population density, are leading to a constant increase in mobility needs. Innovative modes of transport in metropolitan areas shall be fast, safe, and efficient and complement the existing urban transportation systems, sustaining commuters' needs in linking cities and regions. A compelling alternative to ground transportation in overcrowded metropolitan areas is Urban Air Mobility (UAM), in the form of self-piloted, fully electric, vertical take-off and landing (eVTOL) aircraft. Recent improvements concerning electric motors and battery technologies, the availability of reliable off-the-shelf avionics components, and advancements in lightweight materials have made times mature for a new personal short-range concept of aviation. Currently, the interest of key players in the eVTOL market is devoted to unconventional designs entailing a distributed electric propulsion, i.e., multirotor architectures [1, 2], and layouts combining multiple wings, as shown by the Airbus Vahana in Fig. 1. Nevertheless, even if the investigated eVTOLs configurations present very different designs, a key common feature is the multiple propellers architecture, entailing an array of engines positioned over single or dual lifting surfaces, in side-by-side or tandem configurations. These disruptive concepts introduce new challenges in every aspect of the design process, from propulsion to aerodynamics, from aeroacoustics to flight control. Moreover, the design of eVTOL aircraft demands engineers to predict performances, stability, and handling qualities within the entire flight envelope. From an aerodynamic standpoint, eVTOLs introduce new challenges also due to the concurrence of several interactional effects. These effects, e.g., interaction among fixed lifting wings, multirotor interaction, and wake-body interactions, were usually well separated in common aircraft architectures. In eVTOL applications, interactional effects between multiple propellers directly influence the aircraft performances, handling qualities and generate noise. As a matter of fact, there is a certain lack of literature concerning the thorough investigation of such complex aerodynamics within the whole eVTOLs flight envelope.

In particular, the noise impact is essential to the certification process since eVTOL missions mainly concern urban areas. Recent literature reports just a few works concerning rotor-rotor aerodynamic interaction with application to UAV or small drones, e.g., [3, 4]. While the industry is challenged in building commercially viable aircraft, academia is endowed with the quest to fill the knowledge gap concerning the complex aerodynamic and aeroacoustics of multi-rotor systems. Namely, provide accurate and validated tools for devising high-performance aircraft fulfilling strict noise impact requirements. This effort could lead to expressing the full potential of eVTOLs, accelerating their success.

The present work aims to develop an innovative multi-fidelity framework for characterizing the aerodynamics and the aeroacoustics of multirotor systems with application to advanced eVTOL aircraft. Multi-fidelity methods leverage the

Fig. 1 Multi-propellers configuration on eVTOL Airbus Vahana layout (courtesy of A^3 by Airbus LLC).

Table 1 Summary of the test conditions used for numerical validation. The values of L_x/R and L_y/R only hold for the tandem test case.

Symbol	Value	Unit
J	0.8	-
Ω	7050	RPM
β	26.5	$^\circ$
θ	294.05	K
ρ	1.18	$\mathrm{kg\,m^{-3}}$
L_x/R	5	-
L_y/R	0 - 1	-

concatenation of data sets, presenting enormous diversity in terms of information, size, and cost. Pieces of information of diverse fidelity and complexity complement each other, leading to improved prediction accuracy. This approach represents an innovative method successfully employed in very recent applications of multi-rotor aerodynamics, e.g. [5]. As a matter of fact, systematic access to expensive high-fidelity data is still not affordable within the design process of eVTOL aircraft. Parsimony must be pursued, limiting the employment of high-fidelity methods to only a few detailed aerodynamic analyses of particularly interesting configurations. Currently, designers of novel VTOL aircraft are forced to rely on approaches endowed with a low-to-medium fidelity, representing a reasonable trade-off between cost and accuracy. In this framework, the present paper described a multi-fidelity investigation of the aerodynamics and aeroacoustics of two propellers in tandem with overlap, a typical feature of eVTOL architectures. In particular, mid-fidelity aerodynamic simulations are performed using DUST, a vortex particle method (VPM) based open-source solver developed by Politecnico di Milano (POLIMI) in collaboration with A^3 by Airbus [6]. In contrast, high-fidelity CFD simulations are performed using the open-source multi-physics SU2 solver [7]. The final goal of the work is to investigate and compare the capabilities of the two aerodynamic numerical approaches for evaluating the noise footprint of a tandem propeller configuration with different rotor disk overlaps. With this aim, the Ffowcs Williams–Hawkings (FWH) equation solver coupled to both the mid- and high-fidelity simulations output is used to compute the aeroacoustic footprint of the test case in different configurations.

II. POLIMI Tandem Propellers Test Case

The present work considers the tandem propellers experimental configuration designed and tested at Politecnico di Milano (POLIMI). The propeller was designed using a three-bladed hub equipped with left-handed VarioProp 12C blades, thus resulting in a propeller disk diameter D equal to 300 mm. A 65 mm diameter aluminium spinner was screwed on the propeller hub, while a polycarbonate nacelle with 270 mm length was manufactured using the FDM technique to shield the driving system and the load cell. The propeller model geometry is available thanks to a 3D scanning of the blades, while nacelle and spinner geometries were designed and manufactured by one of the authors. The two propellers were arranged in tandem configuration, with an axial distance L_x between the propellers disk equal to 5 rotor radii R. Wind tunnel test conditions consisted of runs performed with tandem co-rotating clockwise propellers with the rotational speed of both propellers controlled to 7050 RPM. This RPM target value was considered to reproduce a typical tip Mach number, i.e., $M_t = 0.325$, of full-scale eVTOL aircraft propellers in cruise flight conditions. Several lateral separation distances L_y between propellers' rotation axis were considered during the experiments to investigate the effects of the degree of overlapping between propeller disks on the rear propeller performance. Test data considered in the present work are summarized in Tab. 1. Propellers' thrust and torque as well as the velocity field are available from experiments for comparison. Indeed, an internal aluminium frame was designed to support the propeller driving system and a bi-axial strain gauge load cell. One of the propeller models was equipped with a Hall-effect sensor that was mounted on the metallic plate below the motor. The Hall-effect sensor was used during the tests to provide the 1/rev signal for the measurement of propeller rotational speed and to trigger the phase-locked stereo Particle Image Velocimetry (PIV) measurements. A detailed description of the experiments is provided in [8]. The layout of the experimental propeller model and the wind tunnel setup are shown in Fig. 2.

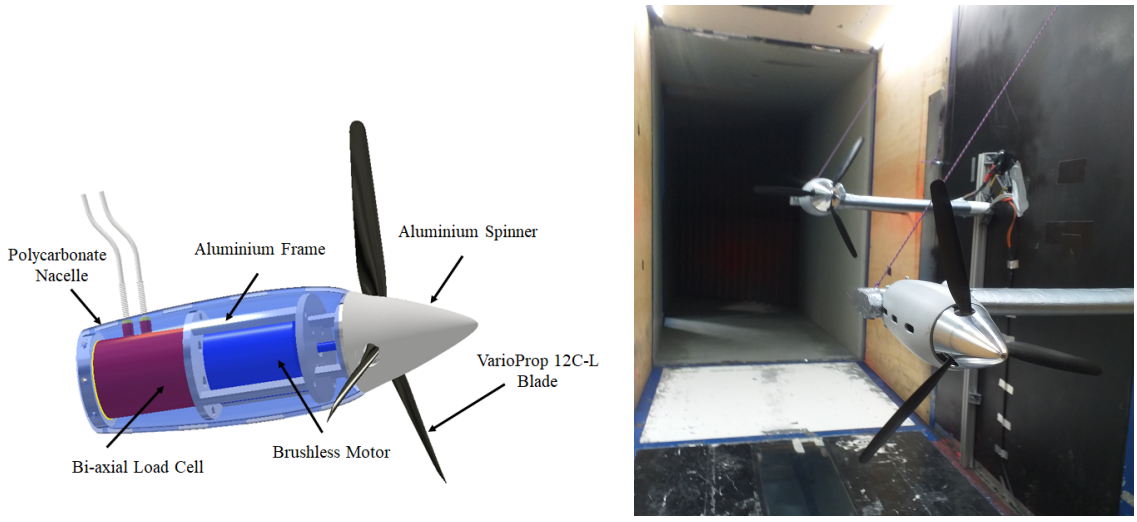

Fig. 2 Layout of the experimental propeller model (a) and of the tandem propellers set up at *S. De Ponte* wind tunnel of POLIMI.

III. Numerical Methods

The numerical investigation was aimed to simulate the wind tunnel test condition reproducing a typical cruise flight condition of eVTOL, i.e., at advance ratio $J = \frac{U_\infty}{nD} = 0.8$, where U_∞ is the free-stream velocity, n the rotor speed expressed in rev/s, and D the rotor diameter. Numerical simulations considered both the single and the tandem propeller configurations. Two lateral separation distances were considered in the simulations: $L_y/R = 0$ (co-axial) and $L_y/R = 1$. As exposed by the experiments, they represent the configurations characterized by the highest aerodynamic interaction between the front propeller slipstream and rear propeller disk [8]. The co-axial case was simulated with both the mid-fidelity and the high-fidelity solver, respectively DUST and SU2, while the non-co-axial case was simulated with DUST only.

DUST solution is computed by discretizing the blade both with lifting line and surface panel elements. In both cases, the nacelle is discretized with panels. Within the text, the solution obtained with a panel discretization of the full geometry is named DUST-PAN, whereas DUST-LL is referred to the lifting line discretization of the blade. Details about the mathematical formulation of such elements can be found in [6]. Lifting line elements include the representation of viscosity effects by the use of tabulated aerodynamic coefficients of the blade airfoils, thus are preferable to better capture the aerodynamic loads of propellers (see [8]). Nevertheless, being lifting line 1D elements, neither the local pressure on the upper and lower surface of the blades nor the blade geometry (both required for aeroacoustic propagations from solid surfaces) are defined with such a method. On the other hand, surface panels can provide these inputs. Thus, only the aerodynamic output coming from this numerical methodology is considered in the present work for acoustic propagation.

The aeroacoustic signature is computed by solving Ffowcs Williams-Hawkings (FWH) equations. The surface pressure field on the propeller computed with the two solvers is provided as input to the same acoustic module. The module has already been verified and validated with SU2 simulations [9]. Thus, it is used as a reference solution for the aeroacoustic signature computed with mid-fidelity aerodynamics inputs. The comparison is carried out for both the isolated propeller and the tandem co-axial propellers ($L_y/R = 0$). After the validation, the aeroacoustics of the tandem configuration with $L_y/R = 1$ is computed by using the mid-fidelity aerodynamic input.

A. DUST: Mid-fidelity Aerodynamic Simulations

DUST is an open-source software developed by Politecnico di Milano since 2017 to simulate the interactional aerodynamics of unconventional rotorcraft configurations. The code is released as free software under the open-source MIT license (`https://www.dust-project.org/`). The code relies on an integral boundary element formulation of the aerodynamic problem and on a vortex particle model [10, 11] of the wakes. This choice naturally fits the Helmholtz

decomposition of the velocity field from a mathematical point of view and avoids the numerical instabilities occurring with connected models of the wake in practice. A numerical model in DUST can be built using several components connected to user-defined reference frames, whose position and motion can be defined hierarchically. Different aerodynamic elements allow for different model fidelity levels, ranging from lifting line elements to zero-thickness lifting surfaces and surface panels for thick solid bodies. In particular, lifting line elements naturally represent viscous effects since they rely on tabulated aerodynamic lift, drag, and moment coefficients of two-dimensional sections as functions of the relative velocity direction and magnitude. The simulation is evolved in time with a time-stepping algorithm, solving in sequence the Morino-like problem [12] for the potential part of the velocity field, the nonlinear problem for the lifting lines, and updating the rotational component of the velocity field integrating the Lagrangian dynamical equations of the wake particles. A detailed mathematical description of the formulation implemented in DUST is reported in [6]. Due to the lower computational costs required for simulations as opposed to high-fidelity CFD simulations based on Navier-Stokes solvers, these mid-fidelity aerodynamic tools were also suitable to be coupled with structural solvers to obtain a fast aeroelastic solution for rotorcraft configurations [13].

B. SU2: High-fidelity Aerodynamic Simulations

SU2 is an open-source software suite initiated at the Aerospace Design Laboratory of Stanford University, freely available and licensed under the GNU Lesser General Public License. It uses the finite volume approach to solve partial differential equations (PDE) on unstructured meshes. It employs a vertex-based approach in contrast to a cell-based method, in which the variables are established and stored at the vertices (nodes). This method utilizes a median-dual grid. It solves the Unsteady Reynold-averaged Navier-Stoke (URANS) equations to analyze typical aeronautical problems that involve turbulent flows in the compressible regime. Concerning flux discretization, various techniques are available, notably JST, ROE, AUSM, Lax-Friedrichs, and HLLC. Second-order precision is attained using a Monotone Upstream-centered Schemes of Conservation Laws (MUSCL) method with gradient limiting. At each grid node, the gradients of the flow variables are calculated using either the least-squares or Green-Gauss method to determine the gradients at the cell faces. The one equation Spalart-Allmaras (SA) and the two equations Menter Shear Stress Transport (SST) turbulence models are implemented in SU2. A dual time-stepping method is used to discretize URANS equations in time. SU2 has also been extensively used for rotorcraft simulations [14]. In the Workshop for Integrated Propeller Prediction, SU2 has been used to model the turbulent flow field around a wing-tip mounted propeller design [15]. An interesting feature is the possibility of recasting the flow equations in a rotating reference system. The reference frame is rotating while the body is fixed in space. The computational cost of the CFD simulation is significantly lowered since this transformation enables the computation of a steady solution to a problem that was unsteady in the inertial frame. This is possible for some specific engineering problems, such as an isolated propeller, where a single object rotates at a constant speed.

C. FWH Noise Computation

In this work, a hybrid CFD-FWH method is presented to predict the far-field tonal noise since it is well known that directly computing the far-field noise for turbulent flows is computationally prohibitive [16]. Indeed, at low Mach number, the acoustic length (λ) scales as $\frac{\lambda}{l} \sim \frac{1}{M}$ [17] when compared to the integral length scale. Two CFD solvers with different levels of fidelity compute the flow variables in the near-field noise source area. Then, a separated module coupled with both codes propagates to a far observer position the acoustic perturbation using a cheaper wave equation. The so-called "wind tunnel configuration", where the source and the observer do not change their relative position, is solved with the integral formulation Kirchhoff or Ffowcs Williams-Hawkings [18] with a computational cost independent of observer distance. Specifically, the implemented formulation was proposed by Di Francescantonio, which combines the positive aspect of the Kirchhoff and FWH equations. The differential equation is reported here:

$$\Box^2 \left[c^2(\rho - \rho_0)\right] = \frac{\partial}{\partial t}\left[\rho_0 U_n \delta(f)\right] - \frac{\partial}{\partial x_i}\left[L_{ij} n_j \delta(f)\right] + \frac{\partial T_{ij}}{\partial x_i, x_j} \tag{1}$$

with:

$$U_i = u_i + (\frac{\rho}{\rho_0} - 1)(u_i - v_i) \tag{2}$$

$$L_{ij} = P'_{ij} + \rho u_i (u_j - v_j) \tag{3}$$

where f is the discontinuity surface, $\Box^2$ the wave operator, T_{ij} is the Lighthill's stress tensor and P'_{ij} is the perturbation stress tensor. Compared to the monopole and dipole terms, quadrupole sources are often insignificant. Therefore the

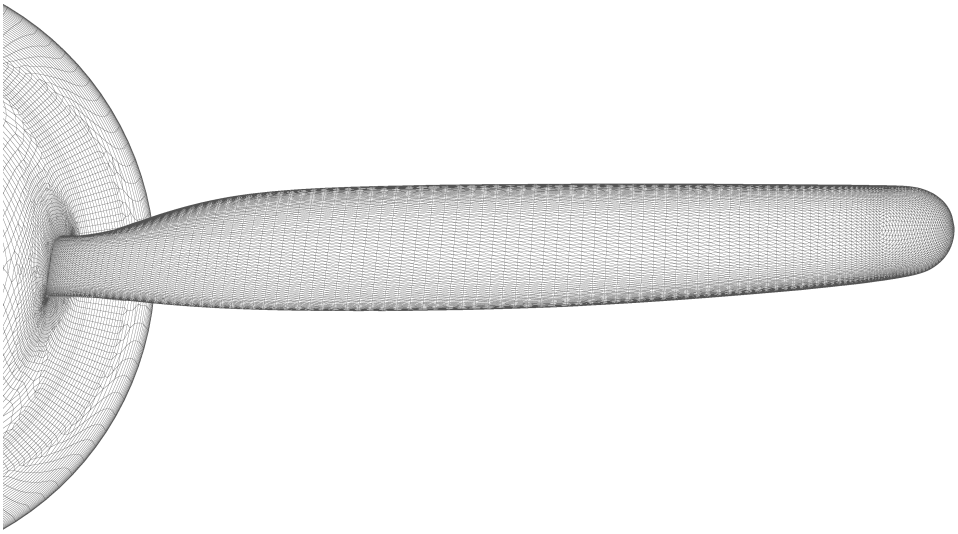

Fig. 3 Surface discretization of the blade (SU2, medium grid)

volumetric sources are neglected, drastically reducing the computational cost. A general moving noise source can be analyzed; both permeable and solid surface versions are coded. However, in this work, only solid surfaces are used, i.e., surfaces where a non-penetration condition is imposed. In this case, the variables of interest are the difference between the local pressure and the free stream one, $p' = P - P_\infty$, and the grid velocity u_n of the surface nodes. The final integral formulation is obtained by applying the Green function approach. Further details can be found in the work by di Francescantonio [19]. The acoustic module has already been verified and validated in [9].

IV. Results and Discussion

The multi-fidelity framework is tested by comparing experimental results with SU2 and DUST over the single propeller test case that was simulated with both codes. The comparison is shown in terms of power and thrust coefficients, flow field, and acoustic signature. The thrust coefficient C_T and power coefficient C_P are defined as follows:

$$C_T = \frac{T}{\rho n^2 D^4} \tag{4}$$

$$C_P = \frac{P}{\rho n^3 D^5} \tag{5}$$

where T is the thrust, P is the power, and ρ is the free-stream air density.

The SU2 simulations are carried out by solving compressible steady RANS equations with a rotating reference frame (RRF) approach. Spalart-Allmaras turbulence model [20] was used with the algebraic BCM transition model [21] considering a freestream turbulence intensity of 0.1%. Convective fluxes were solved using JST numerical scheme with 0.5 and 0.005 as 2^{nd} and 4^{th} order dissipation coefficients, respectively. The gradients of the variables at each node were reconstructed using the Green-Gauss theorem. The domain was discretized using Pointwise. Grid convergence was checked on the isolated propeller test case using a set of three different grids consisting of 6.9×10^6, 18.0×10^6, and 56.6×10^6 cells each. The grids will be referred to as Coarse, Medium, and Dense. They had a maximum y^+ value at the first cell in the normal direction of 2.5, 1.8, and 1.2, respectively. A close-up view of the blade surface discretization of the Medium grid is shown in Fig. 3. For the tandem configuration, the same surface discretization of the medium grid was applied to both propellers. To avoid excessive dissipation of the vortices generated by the front propeller, volume elements of 4 mm were applied in its wake region. The grid had a total of 50×10^6 elements. The computational time required to complete the simulation of the tandem propeller co-axial configuration was about 8 h using 8 nodes on an HPC platform, each node consisting of 2× AMD EPYC^{TM} 7742 @2.25 GHz processors with 64 cores for each processor.

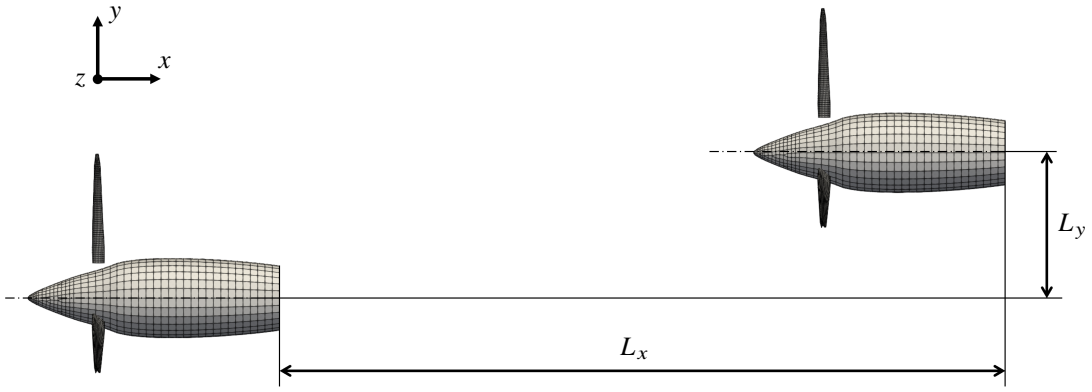

Fig. 4 Layout of the tandem propellers model mesh built for DUST simulations.

DUST numerical model of the propellers (see Fig. 4) was built using both lifting lines elements and surface panels for the three blades, while surface panels were used to model the spinner-nacelle surface. Simulations were carried out considering a total of 10 propeller revolutions with a time discretization corresponding to 128 steps for each complete revolution. A fully developed wake for the interacting propellers test cases comprised around one million vortex particles. The computational time required to complete the simulation of the tandem propeller configuration was about 130 minutes using a workstation with a Dual Intel® Xeon Gold 6230R @2.10GHz processor with 52 physical cores and 2 threads for each core.

A. Isolated Propeller

The results of mid- and high-fidelity simulations are first compared with experimentally measured torque and power coefficients and with the PIV-measured flow field. The results are provided in terms of thrust coefficient C_T and power coefficient C_P. Their values are shown in Table 2, including all three grids of RANS simulations for grid convergence analysis. A quite good agreement with experimental results is found with both SU2 and DUST-LL, with SU2 simulations being slightly more accurate. DUST-PAN simulations provide a higher discrepancy with experimental results. Regarding the grid convergence of SU2 simulations, for both coefficients, the relative error between the Coarse and the Medium grids and between the Medium and the Dense grids is below 1% and 0.5%, respectively. Thus, from now on, the Medium grid will be considered for the SU2 results.

PIV measurements are then considered for comparison. The experimental acquisition was phase-locked considering an azimuth angle $\psi = 170°$ with respect to the reference blade, as shown in Fig. 5. The phase-averaged value of the vertical component of the velocity field (u_y) is compared with numerical simulations in Fig. 6. The same region of the PIV-measured flow field is shown. In this case, all numerical simulations show good agreement with the experimental measurements, including the flow field computed with DUST using a surface panel discretization of the blade.

Table 2 Thrust coefficient C_T and power coefficient C_P (isolated propeller).

Solution	C_T	C_P
DUST-LL	0.106	0.113
DUST-PAN	0.166	0.159
SU2 (Dense)	0.097	0.111
SU2 (Medium)	0.097	0.111
SU2 (Coarse)	0.096	0.110
Experiment	0.101	0.107

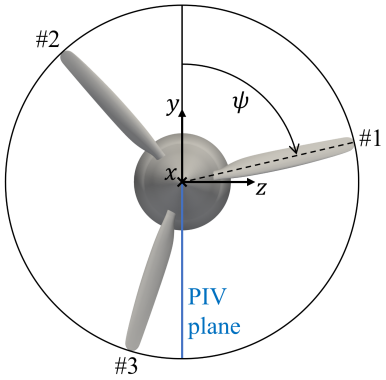

Fig. 5 Definition of blade azimuth angle ψ. PIV acquisition occurs at $\psi = 170°$.

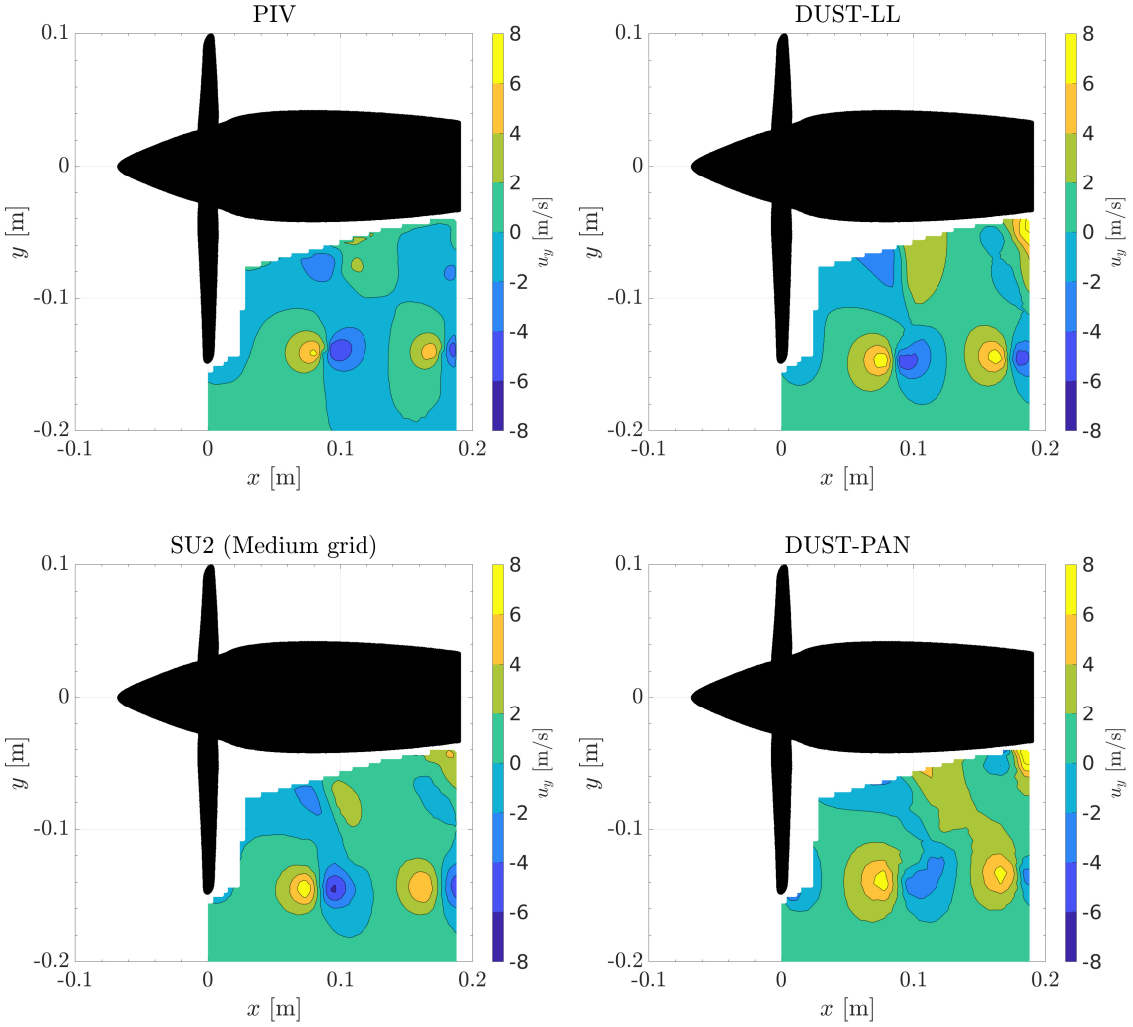

Fig. 6 Vertical component of the velocity field. Top left: PIV measurements. Bottom left: SU2 simulation. Top right: DUST simulation with lifting line blade. Bottom right: DUST simulation with surface panel blade.

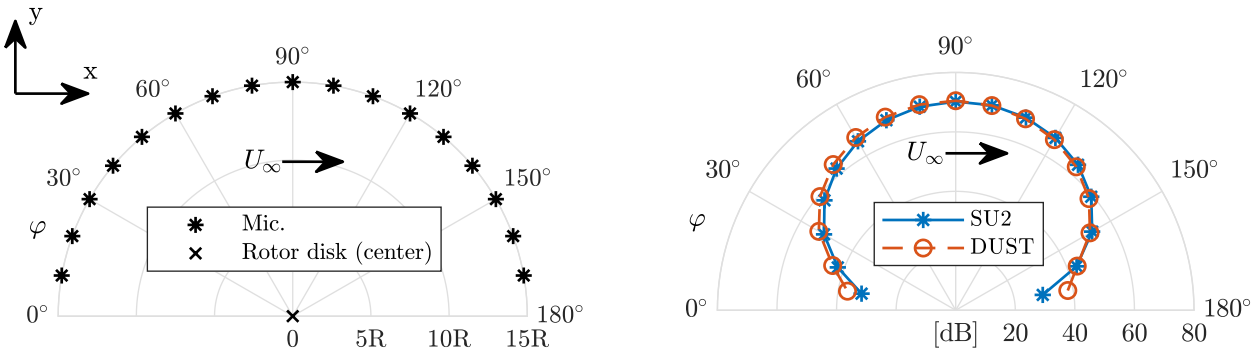

Fig. 7 Isolated propeller. Left: position of the microphone array. Right: SPL comparison.

The solutions obtained with DUST using surface panels and with SU2 using the medium grid are now used to compute the tonal noise emitted by the propeller. The FWH integral formulation, in the solid surface version, propagates the acoustic perturbation to 19 microphones equally positioned from $\varphi = 10°$ to $\varphi = 170°$ at a Euclidean distance of fifteen times the blade radius. The so-called "wind tunnel configuration" is simulated in the reference system shown in Fig. 7. The Sound Pressure Level (SPL) in dB is shown in Fig. 7 and reported in Tab. 3. It is computed according to the following formula:

$$\mathrm{SPL[dB]} = 20 \log_{10} \left(\frac{p'_{\mathrm{rms}}}{20 \times 10^{-6}} \right), \tag{6}$$

where p'_{rms} is the mean root average of the acoustic pressure fluctuation at each observer over a time T:

$$p'_{\mathrm{rms}} = \sqrt{\frac{1}{T} \int_0^T p'(t)^2 \, dt}. \tag{7}$$

The value obtained with the SU2 solution is taken as the reference one, as already validated by [9]. The maximum difference between the SPL computed by the two different approaches is slightly higher than 1%. Thus, the mid-fidelity solution provided by DUST obtained over a quite lower computational effort with respect to the high-fidelity approach is suitable for evaluating the acoustic signature of a propeller in airplane mode flight conditions.

Table 3 SPL comparison in dB (isolated propeller).

Mic. φ	10°	20°	30°	40°	50°	60°	70°	80°	90°
DUST-PAN	38.20	43.40	52.05	58.39	62.96	66.25	68.52	69.91	70.47
SU2	32.09	42.12	51.03	57.51	62.20	65.61	68.01	69.53	70.19
Mic. φ	170°	160°	150°	140°	130°	120°	110°	100°	
DUST-PAN	36.89	43.95	53.05	59.47	63.97	67.09	69.13	70.22	
SU2	29.66	43.18	52.88	59.39	63.86	66.93	68.94	70.00	

B. Tandem Propellers: Co-Axial

In this section, two propellers are positioned with a horizontal separation of $L_x/R = 5$ and no vertical distance $L_y/R = 0$, taking as reference Fig. 4. The free-stream conditions are the same as the isolated propeller. The simulations are conducted both with DUST using surface panels and with SU2 with a rotating reference system. The loads are compared with wind tunnel measurements. In particular, the loss of thrust and torque of the rear propeller with respect to the isolated one is reported in Tab. 4.

Concerning the mid-fidelity solver, the data clearly underline that the lifting line method better predicts the loads with respect to the panel one. However, only the surface data extracted with the less accurate approach can be used with

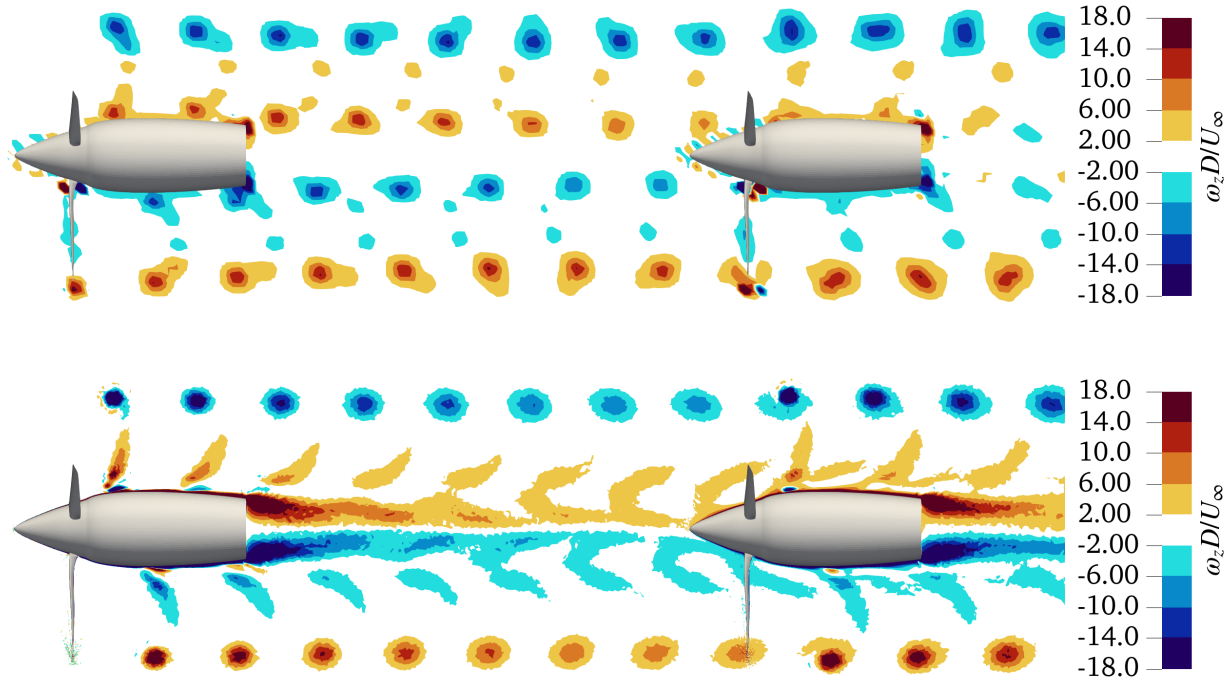

Fig. 8 Contour plot of the out-of-plane component of the non-dimensional vorticity $\omega_z D/U_\infty$. Top: DUST (panels). Bottom: SU2 (RRF-RANS).

the FWH solid surface formulation. Fig. 8 compares the out-of-plane component of the non-dimensional vorticity $\omega_z D/U_\infty$ obtained with the SU2 and the DUST-PAN solutions. While the wake of the nacelle acting as a bluff body is not well captured as expected by the mid-fidelity solver, a good analogy can be observed for the blade tip vortices' evolution. The particle-wake method used by DUST perfectly conserves the vortices, while the finite-volume approach of SU2 leads to some dissipation. The loss of thrust computed with SU2 is in good agreement with the wind tunnel data, while DUST-PAN overpredicts the value.

Noise emission is computed at 17 microphones equally distributed on an arch from $\varphi = 10°$ to $\varphi = 170°$, with a step of 10°. The arch is centred at the middle point between the two propellers and has a radius of $10R + 0.5L_x$, as shown in Fig. 9. The resulting SPL is reported in the same figure as well as in Tab. 5. The p' is computed considering as sources 128 surface flow solutions per period of revolution. In this case, some differences can be appreciated in the sound pressure level computed with the two approaches, especially for the microphones closer to the axis of rotation. To further analyse the difference in the results of the co-axial tandem configuration, the SPL was computed by considering as input of the acoustic propagation the surface pressure distribution of each propeller separately. The results are shown in Fig. 10. By considering the front propeller only, results are qualitatively similar to the isolated propeller test case. As expected, some minor differences between DUST and SU2 are present, slightly increasing closer to the rotation axis, as

Table 4 Loss of thrust and power of the rear propeller with respect to the isolated one. $L_y = 0R$.

Solution	ΔC_T	ΔC_P
DUST-LL	-33 %	-22%
DUST-PAN	-53 %	-47.3%
SU2	-31.3 %	-19.6 %
Experiment	-29.7 %	-21.3 %

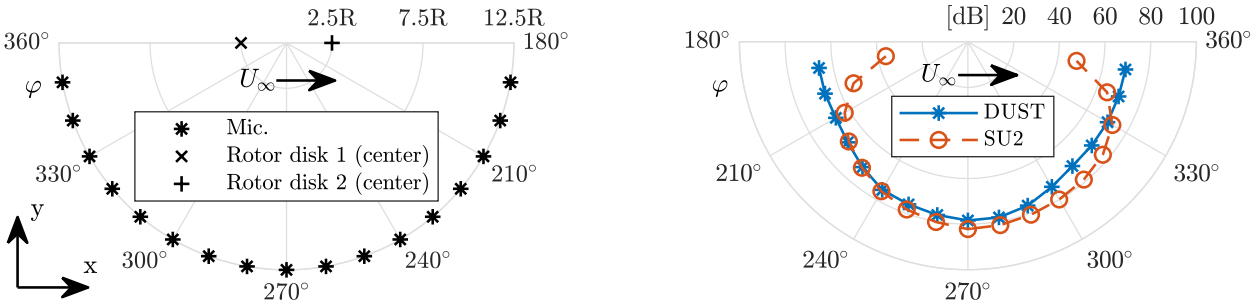

Fig. 9 Co-axial tandem. Left: position of the microphone array. Right: SPL comparison.

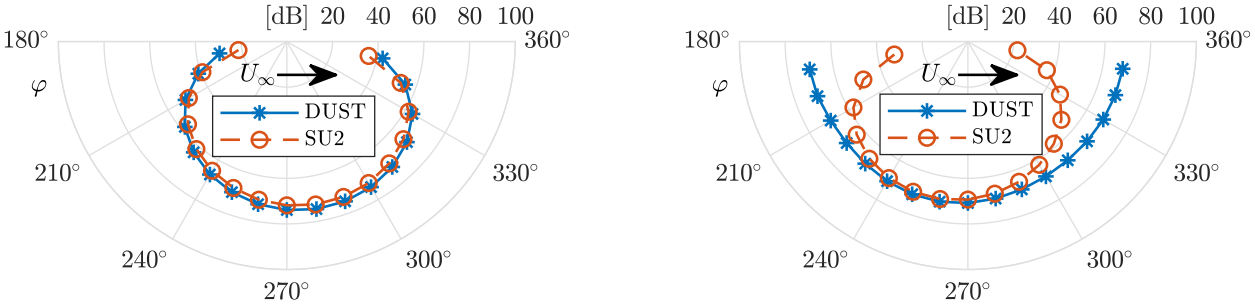

Fig. 10 Co-axial tandem, considering one propeller at a time as sound source. Left: front propeller. Right: rear propeller.

occurred for the isolated propeller. Once more, the characteristic shape of a dipole source is recovered. It can also be noticed that the upwind microphones recorded a SPL higher than the downwind ones, being closer to the propeller. On the other hand, by considering the rear propeller only, differences become higher, especially getting closer and closer to the rotation axis. In this case, by providing the less accurate solution in terms of loads obtained with surface panels as input, the characteristic shape of the dipole solution that was found in all other simulations is not captured.

Table 5 SPL comparison in dB (Co-axial tandem).

Mic. φ	190°	200°	210°	220°	230°	240°	250°	260°	270°
DUST-PAN	66.16	66.55	66.74	68.64	71.76	75.00	75.91	77.15	78.38
SU2	36.46	53.26	62.26	68.01	72.15	75.71	78.29	80.29	82.18
Mic. φ	350°	340°	330°	320°	310°	300°	290°	280°	
DUST-PAN	70.03	70.18	70.58	70.76	71.16	73.48	76.49	78.24	
SU2	48.28	64.84	73.00	77.10	78.93	79.89	80.73	81.67	

C. Tandem Propellers: Vertical Separation

Due to its computational efficiency, the mid-fidelity DUST solver is used to investigate the effect of vertical separation between the two propellers, taking into analysis the aerodynamic performance and the noise emitted. The configuration with L_y = 1R is chosen and compared with the co-axial one. The free-stream conditions are the same as the other test cases. This configuration had been tested in the wind tunnel as well. A visualization of the vortices identified through the Q-criterion in the DUST simulations is provided in Fig. 11.

For the noise computation, two sets of microphone arrays are considered. They are shown in Fig. 12, and they all belong to the xy plane shown in Fig. 4. The first array of 10 microphones is centered in the rotor disk of the front propeller, is placed at $10R$ distance, and covers an amplitude of $-90°$ to $90°$ in front of the rotor. The second array of 10

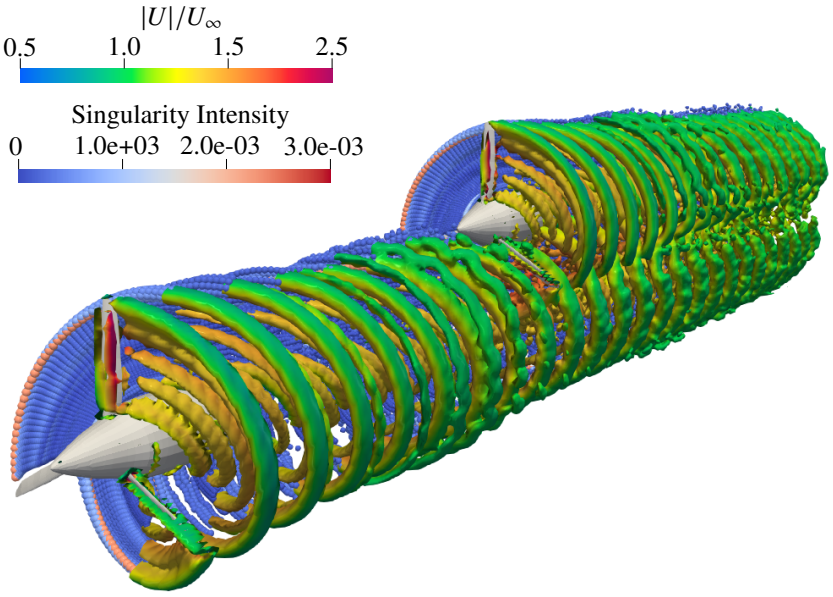

Fig. 11 Visualization of the flow field (Q-criterion iso-surface colored by non-dimensional freestream velocity) and particles wake (colored by singularity intensity) computed by DUST. Tandem propellers configuration, $L_x = 5R$ and $L_y = 1R$.

Table 6 Loss of thrust and power of the rear propeller with respect to the isolated one. $L_y = 1R$.

Solution	ΔC_T	ΔC_P
DUST-PAN	−4.4 %	−1.6 %
Experiment	−5.2 %	−3.8 %

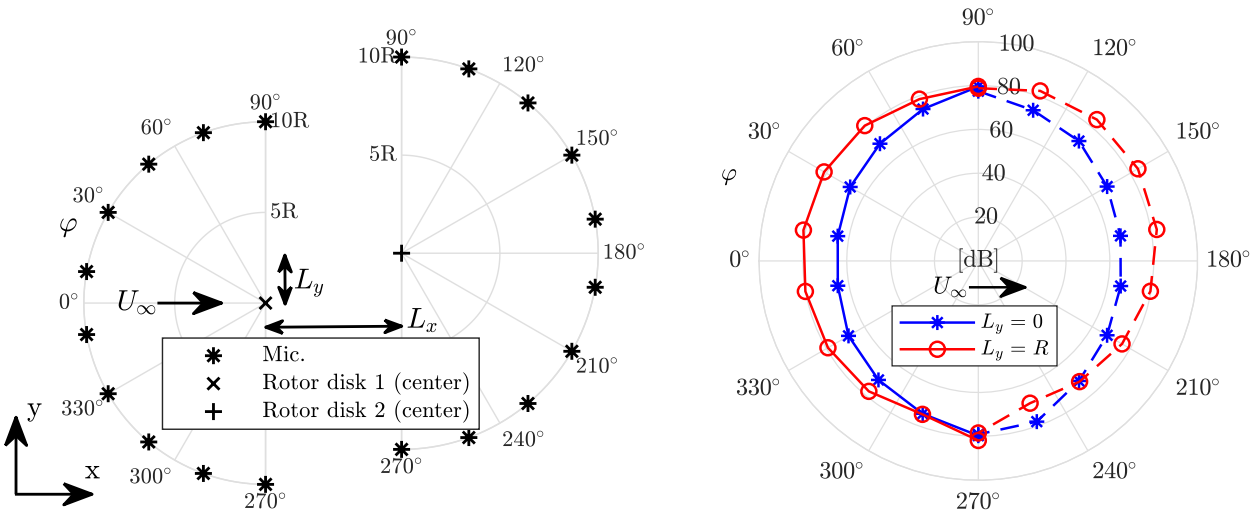

Fig. 12 Tandem with vertical separation. Left: microphone array position. Right: SPL comparison (DUST only).

microphones is centered in the rotor disk of the rear propeller, is placed at $10R$ distance, and covers an amplitude of 90° to 270°, downwind. The configuration is sketched in Fig. 12.

Introducing a vertical separation between the propellers generates an advantage with respect to the co-axial configuration in terms of the overall thrust coefficient, which is confirmed both by the numerical simulations and the experiments (Tab. 6). In contrast, concerning noise, all microphones of both the front and back arch perceive a lower SPL if the co-axial configuration is chosen, as shown in Fig.12. The following result is sustained by the spectral analysis of the time history of the loads measured in the wind tunnel for the rear propeller, where the amplitude of the thrust peaks are lower for the co-axial test case (see [8]).

V. Conclusions

The present work is aimed at performing a multi-fidelity numerical assessment of the aeroacoustics of a tandem propeller configuration typical of an eVTOL aircraft in airplane mode flight conditions. Tonal noise was analyzed by solving the FWH equations using the formulation by di Francescantonio [19]. The validation of the aeroacoustic formulation using the aerodynamics input coming from the high-fidelity simulations had already been carried out for an isolated propeller [9]. This work proved that the mid-fidelity approach implemented in DUST can provide accurate acoustic prediction at very low computational effort.

The acoustic signature of the geometry was computed by providing as input for sound propagation the surface pressure field coming from two different solvers. For high-fidelity simulations, RANS equations were solved in SU2 using a rotating reference frame approach. For mid-fidelity simulations, surface panels were used as aerodynamic elements in the vortex-particle-method-based code DUST. Such elements do not provide an accurate prediction of the loads on the propellers, but permit a straightforward application of the solid surface FWH formulation with good accuracy of the acoustic footprint with respect to the one evaluated with high-fidelity CFD input.

Concerning an isolated propeller case, the discrepancy in the aerodynamic loads was not reflected in the noise computed. The acoustic fluctuations predicted from the mid-fidelity solution matched almost perfectly the solution generated with a high-fidelity input. This highlights the suitability of the DUST mid-fidelity approach for the aeroacoustic investigation of such test-case at a fraction of the computational cost required by high-fidelity CFD simulations. On the other hand, the co-axial tandem test case showed some differences between the two approaches in the sound pressure level computed. It was shown that the difference is mainly due to the contribution given by the rear propeller to noise emission. This result highlights the necessity of coupling the FWH formulation with the lifting line model of DUST, to provide an even faster, more comprehensive, and possibly more accurate approach for tonal aeroacoustics predictions. In the end, a vertical separation was introduced between the two propellers, showing an advantage in terms of aerodynamic performance for the rear propeller performance and, in contrast, an increase in noise emittance.

Acknowledgments

The present work is done in the framework of the GARTEUR Action Group RC/AG-26 *Noise Radiation and Propagation for Multirotor System Configurations*. The authors gratefully acknowledge the high performance computing resources provided for this collaborative effort by the UK National Supercomputing Service via ARCHER2 (http://www.archer2.ac.uk), on Project e734 (High-Fidelity Aerodynamic and Aeroacoustic Simulations for Urban Air Mobility Concepts). G. Gori would like to acknowledge that this work was partially funded by the European Union (Project 101059320 - UN-BIASED). Views and opinions expressed are however those of the author(s) only and do not necessarily reflect those of the European Union or the European Research Executive Agency. Neither the European Union nor the European Research Executive Agency can be held responsible for them.

References

[1] Polaczyk, N., Trombino, E., Wei, P., and Mitici, M., "A Review of Current Technology and Research in Urban On-Demand Air Mobility Applications," *Proceedings of the Vertical Flight Society's 6th Annual Electric VTOL Symposium*, Mesa, AZ, USA, 2019.

[2] Silva, C., Johnson, W., Solis, E., Patterson, M. D., and Antcliff, K. R., "VTOL Urban Air Mobility Concept Vehicles for Technology Development," *Proceedings of the 2018 Aviation Technology, Integration, and Operations Conference*, AIAA, Atlanta, GA, USA, 2018. https://doi.org/10.2514/6.2018-3847.

[3] Zhou, W., Ning, Z., Li, H., and Hu, H., "An Experimental Investigation on Rotor-to-Rotor Interactions of Small UAV Propellers," *Proceedings of the 35th AIAA Applied Aerodynamics Conference*, Denver, USA, 2017. https://doi.org/10.2514/6.2017-3744.

[4] Shukla, D., and Komerath, N., "Multirotor Drone Aerodynamic Interaction Investigation," *Drones*, Vol. 2, No. 4, 2018, pp. 1–13. https://doi.org/10.3390/drones2040043.

[5] Pinti, O., Oberai, A. A., Healy, R., Niemiec, R. J., and Gandh, F., "Multi-Fidelity Approach to Predicting Multi-Rotor Aerodynamic Interactions," *AIAA Journal*, Vol. 60, No. 6, 2022, pp. 3894–3908. https://doi.org/10.2514/1.J060227.

[6] Tugnoli, M., Montagnani, D., Syal, M., Droandi, G., and Zanotti, A., "Mid-fidelity approach to aerodynamic simulations of unconventional VTOL aircraft configurations," *Aerospace Science and Technology*, Vol. 115, 2021, p. 106804. https://doi.org/10.1016/j.ast.2021.106804.

[7] Economon, T. D., Palacios, F., Copeland, S. R., Lukaczyk, T. W., and Alonso, J. J., "SU2 An open-source suite for multiphysics simulation and design," *AIAA Journal*, Vol. 54, No. 3, 2016, pp. 828–846. https://doi.org/10.2514/1.J053813.

[8] Zanotti, A., and Algarotti, D., "Aerodynamic interaction between tandem overlapping propellers in eVTOL airplane mode flight condition," *Aerospace Science and Technology*, Vol. 124, 2022, p. 107518. https://doi.org/10.1016/j.ast.2022.107518.

[9] Galimberti, L., Morelli, M., Guardone, A., and Zhou, B. Y., "Propeller Noise Prediction Capabilities within SU2," *Proceedings of the AIAA SCITECH 2023 Forum*, National Harbor, MD & Online, 2023, p. 1548. https://doi.org/10.2514/6.2023-1548.

[10] Winckelmans, G. S., "Topics in vortex methods for the computation of three-and two-dimensional incompressible unsteady flows," Ph.D. dissertation, California Institute of Technology, 1989. https://doi.org/10.1016/j.crhy.2005.05.001.

[11] Cottet, G. H., and Koumoutsakos, P. D., *Vortex methods: theory and practice*, Cambridge University Press, 2000.

[12] Morino, L., and Kuo, C.-C., "Subsonic Potential Aerodynamics for Complex Configurations: A General Theory," *AIAA Journal*, Vol. 12, No. 2, 1974, pp. 191–197. https://doi.org/10.2514/3.49191.

[13] Savino, A., Cocco, A., Zanotti, A., Tugnoli, M., Masarati, P., and Muscarello, V., "Coupling Mid-Fidelity Aerodynamics and Multibody Dynamics for the Aeroelastic Analysis of Rotary-Wing Vehicles," *Energies*, Vol. 14, No. 21, 2021, p. 6979. https://doi.org/10.3390/en14216979.

[14] Morelli, M., Bellosta, T., and Guardone, A., "Development and preliminary assessment of the open-source CFD toolkit SU2 for rotorcraft flows," *Journal of Computational and Applied Mathematics*, Vol. 389, 2021, p. 113340. https://doi.org/10.1016/j.cam.2020.113340.

[15] Zhou, B. Y., Morelli, M., Gauger, N. R., and Guardone, A., "Simulation and Sensitivity Analysis of a Wing-Tip Mounted Propeller Configuration from the Workshop for Integrated Propeller Prediction (WIPP)," *Proceedings of the AIAA AVIATION 2020 FORUM*, virtual event, 2020. https://doi.org/10.2514/6.2020-2683.

[16] Colonius, T., and Lele, S. K., "Computational aeroacoustics: progress on nonlinear problems of sound generation," *Progress in Aerospace sciences*, Vol. 40, No. 6, 2004, pp. 345–416. https://doi.org/10.1016/j.paerosci.2004.09.001.

[17] Sarkar, S., and Hussaini, M. Y., "Computation of the Acoustic Radiation from Bounded Homogeneous Flows," *Computational Aeroacoustics*, edited by J. C. Hardin and M. Y. Hussaini, Springer New York, New York, NY, 1993, pp. 335–355. https://doi.org/10.1007/978-1-4613-8342-0_21.

[18] Farassat, F., "Linear Acoustic Formulas for Calculation of Rotating Blade Noise," *AIAA Journal*, Vol. 19, No. 9, 1981, pp. 1122–1130. https://doi.org/10.2514/3.60051.

[19] Di Francestantonio, P., "A new boundary integral formulation for the prediction of sound radiation," *Journal of Sound and Vibration*, Vol. 202, No. 4, 1997, pp. 491–509. https://doi.org/10.1006/jsvi.1996.0843.

[20] Spalart, P., and Allmaras, S., "A one-equation turbulence model for aerodynamic flows," *Proceedings of the 30th Aerospace Sciences Meeting and Exhibit*, Reno, NV, USA, 1994. https://doi.org/10.2514/6.1992-439.

[21] Cakmakcioglu, S. C., Bas, O., Mura, R., and Kaynak, U., "A Revised One-Equation Transitional Model for External Aerodynamics," *Proceedings of the AIAA AVIATION 2020 FORUM*, virtual event, 2020. https://doi.org/10.2514/6.2020-2706.